Eur. Phys. J. C manuscript No.
(will be inserted by the editor)

Physics potential for the H→ZZ decay at the CEPC

Ryuta Kiuchi[1], Yanxi Gu[2], Min Zhong[2], Lingteng Kong[3], Alex Schuy[4], Shih-Chieh Hsu[b,4], Xin Shi[a,1], Kaili Zhang[1]

[1]Institude of High Energy Physics, Chinese Academy of Science, Beijing 100049, China
[2]Department of Modern Physics, University of Science and Technology of China, Hefei 230026, China
[3]University of Chinese Academy of Sciences, Beijing, 100049, China
[4]Department of Physics, University of Washington, Seattle 98195-1560, USA

Received: date / Accepted: date

Abstract The precision of the yield measurement of the Higgs boson decaying into two Z bosons process at the Circular Electron-Positron Collider (CEPC) is evaluated. Including the recoil Z boson associated with the Higgs production (Higgsstrahlung) total three Z bosons are produced for this channel, from which final states characterized by the presence of a pair of leptons, quarks, and neutrinos are chosen for the signal. Two analysis approches are compared and the final precision of $\sigma_{ZH}\cdot$Br(H→ZZ) is estimated to be 8.80% using a multivariate analysis technique, based on boosted decision trees. The relative precision of the Higgs boson width, using this H→ZZ decay topology, is estimated by combining the obtained result with the precision of the inclusive ZH cross section.

Keywords CEPC · Higgs boson · Higgs to ZZ

1 Introduction

After the discovery of the Higgs boson [1,2], efforts are performed on measuring properties of the Higgs boson. One of motivations of these studies is to obtain hints for physics beyond the Standard Model (SM), whose existence is suggested by several experiment facts, such as dark matter, cosmological baryon-antibaryon asymmetry. The Circular Electron-Positron Collider (CEPC) [3, 4] is a proposed future circular e^+e^- collider, having its main ring circumstance of ∼100 km. As a Higgs factory, the CEPC is planned to operate at $\sqrt{s} = 240$ GeV with the integrated luminosity of $5.6ab^{-1}$ which is expected to achieve an order of magnitude improvement on measurements of Higgs boson properties as compared to the final LHC precision.

[a]e-mail: shixin@ihep.ac.cn
[b]e-mail: schsu@uw.edu

The Higgs production mechanisms at $\sqrt{s} = 240$ GeV will be the Higgsstrahlung process $e^+e^-\rightarrow\mathrm{Z}^*\rightarrow\mathrm{ZH}$ (hereafter, denoted as ZH process) and the vector boson fusion processes, $e^+e^-\rightarrow\mathrm{W}^{+*}\mathrm{W}^{-*}\nu_e\bar{\nu}_e\rightarrow\mathrm{H}\nu_e\bar{\nu}_e$ ($\nu\bar{\nu}$H process) and $e^+e^-\rightarrow\mathrm{Z}^*\mathrm{Z}^*e^+e^-\rightarrow\mathrm{H}e^+e^-$, where the former is dominating over all of the others, therefore, is going to provide series of the Higgs measurements, such as the cross section $\sigma(ZH)$, using the recoil mass method against the Z boson. That Z boson also serves as a tag of the ZH process by identifying decay fermions from it. With this tag information, individual decay channels of the Higgs boson will be explored subsequently and give us valuable information on the Higgs boson properties ever.

The Higgs decay into a pair of Z bosons, via the ZH process, will be studied at the CEPC. Like the other decay modes, the Branching ratio BR(H→ZZ) can be obtained from the measurement of the signal yield, $\sigma(ZH)\times$BR(H→ZZ). In addition, the Higgs boson width Γ_{H} can be inferred as well. Under the assumption that the coupling structure follows to that of the SM, the branching ratio is proportional to the term, $\mathrm{BR(H\rightarrow ZZ)} = \Gamma(\mathrm{H\rightarrow ZZ})/\Gamma_{\mathrm{H}} \propto g^2_{\mathrm{HZZ}}/\Gamma_{\mathrm{H}}$, therefore, Γ_{H} is deduced with the uncertainty coming from the measurement of the coupling g^2_{HZZ} ($\sigma(\mathrm{ZH})\propto g^2_{\mathrm{HZZ}}$) and the signal yield. Note that the vector boson fusion $\nu\bar{\nu}$H process in combination with measurements of final states from H→WW decay will also give the Γ_{H} value and consequently the final value will be determined from the combination of the two measurements[4,5].

The study of H→ZZ channel via the ZH process has an unique feature among the other decays that is originated from its event topology where two on-shell Z bosons and one off-shell Z boson are involved. Considering various Z boson's decay possibilities, the topology diverges into lots of final states. H→ZZ→4l decay is the so-called "golden channel" of the Higgs boson study at the LHC, as it has the cleanest signature of all the possible Higgs boson decay modes. However, the statistics of this leptonic channel at the CEPC may not allow to study the properties with required precision. Conversely, fully hadronic channel can provide enough statistics, but difficulties in identifying and matching jets with proper Z bosons, as well as efficient separation from the SM backgrounds have to be overcome. Between these two extremes, the decay channels having a pair of leptons, jets and neutrinos are most promising candidates for studying H→ZZ properties, owing to its clear signature and larger branching fraction than the leptonic channel. Therefore, this final state has been chosen as the signal for the evaluation of the HZZ properties. Muons have most advantage among charged leptons for discriminating isolated status from those produced by semi-leptonic decays of heavy flavor jets and the final states including a pair of muons are selected as the signal process: Z→$\mu^+\mu^-$, H→ZZ*→$\nu\bar{\nu}q\bar{q}$ (Fig. 1) and its cyclic permutations, Z→$\nu\bar{\nu}$, H→ZZ*→$q\bar{q}\mu^+\mu^-$ and Z→$q\bar{q}$, H→ZZ*→$\mu^+\mu^-\nu\bar{\nu}$, where the q represents all quark flavors except for the top quark.

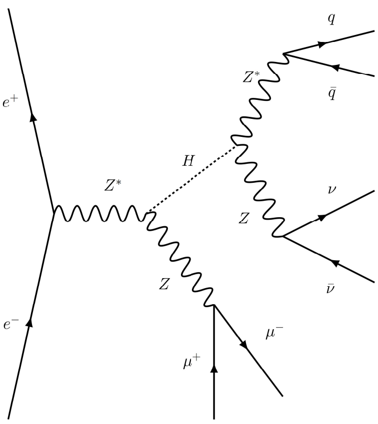

Fig. 1 Example Feynman diagram of the signal process which is characterized by the presence of a pair of muons, jets and neutrinos. In this example, the initial Z boson associated with the Higgs production is decaying into muons whereas cyclic permutation of the decay products from 3 Z bosons is considered in the analysis.

In this article, we report on the estimation of relative accuracy of the yield measurement for the H→ZZ decay at the CEPC using the signal process characterized by the presence of a pair of muons, jets and neutrinos. In Section 2, we briefly introduce the CEPC detector design and the Monte Carlo (MC) simulation scheme. The event selection is described in Sec. 3, followed by an estimation on the precision of the signal yield in Sec. 4. Finally, conclusions are given in Sec. 5.

2 Detector design and simulation samples

The CEPC will hosts two interaction points (IP) on the main ring, where the detectors at each IP should record collision data under different center of mass energies varying from $\sqrt{s} = 91.2$ GeV as a Z factory to $\sqrt{s} = 240$ GeV as a Higgs factory. To fulfill those physics programs, a baseline concept of the detector is developed that is based on the International Large Detector (ILD) concept [6] with further optimizations for the CEPC environment. List it from the most inner sub-detector component, the detector concept is composed of a silicon vertex detector, a silicon inner tracker consisting of micro strip detectors, a Time Projection Chamber (TPC), a silicon external tracker, ultra-fine segmented calorimeters, an Electromagnetic CALorimeter (ECAL) and an Hadronic CALorimeter (HCAL), a 3T superconducting solenoid, and a muon detector [4].

The CEPC simulation software package implements the baseline concept detector geometry. Events for the SM processes are generated by the Whizard [7] including the Higgs boson signal, where the detector configuration and response is handled by the GEANT4-based simulation framework, MokkaPlus [8]. Modules for digitization of the signals at each sub detector creates the hit information. Particle reconstruction has been taken place with the Arbor algorithm, which builds the reconstructed particles using calorimeter and track information[9].

The Higgs boson production and decay are simulated with the scheme, where the generated samples also contain the WW/ZZ fusion processes. All of the SM background samples, which can be classified into 2-fermion processes ($e^+e^-\to f\bar{f}$) and 4-fermion processes ($e^+e^-\to f\bar{f}f\bar{f}$), are produced as well.

3 Event Selection

Event selection is performed in several stages. The preselection builds higher-level objects, such as isolated muons, jets, and missing momentum from the Particle Flow (PF) objects which are reconstructed by the ArborPFA. The isolation requirements on muons, identified by the PFs, are imposed. For muons with energy higher than 3 GeV, tracks inside of a cone with a half-opening angle θ around the candidate are examined and it is identified as an isolated muon, when a ratio between the energy of the muon candidate and a summation of the energy from all of the tracks except for the candidate in a volume defined by the cone is higher than 0.1 with $\cos\theta = 0.98$. Jets are clustered from the PFs but except for isolated lepton candidates, using the k_t algorithm for the e^+e^- collision ($ee - kt$) with the FastJet package. Exclusive requirement ($N_{jet} = 2$) on number of jets is imposed. Events are requested to have a pair of isolated muons of positive and negative charged, and two jets successfully clustered.

The events satisfying the pre-selection criteria are separated into two categories separately for each of 3 final states in the signal process, according to the order of the invariant mass from di-objects which are not forming the tag of the initial Z boson. This categorization, distinguishing between the status having a pair of objects suppose to be decaying from the on-shell Z boson and that from the off-shell Z boson where H→ZZ* decay is assumed, enhances the efficiency of the event selection by applying different selection criteria for each category respectively. Following notation is adopted for each category: $\mu\mu\mathrm{H}\nu\nu qq$ is defined for the events with the reconstructed invariant mass of missing term $M_{\mathrm{miss.}}$ due to escaping neutrinos is larger than that of dijet M_{jj}, where two characters of the top represent a pair of muons decaying from the initial Z boson.

On total 6 exclusive categories, $\mu\mu\mathrm{H}\nu\nu qq$, $\mu\mu\mathrm{H}qq\nu\nu$, $\nu\nu\mathrm{H}\mu\mu qq$, $\nu\nu\mathrm{H}qq\mu\mu$, $qq\mathrm{H}\nu\nu\mu\mu$, $qq\mathrm{H}\mu\mu\nu\nu$, the events have been selected. Two different analysis approches are explored for this stage, the one where requirements are imposed on a set of kinematic variables (referred to "cut-based" analysis) and the one which uses a multivariate analysis technique, based on the boosted decision tree (BDT) implemented within scikit-learn package [11], in order to achieve better separation between signal and background (referred to "'BDT" analysis).

For the cut-based analysis, the signal to background ratio is minimized by following requirements. The invariant mass $M_{\mu\mu}$ of the two muons, the invariant mass M_{jj} of two jets and the missing mass $M_{\mathrm{miss.}}$ are required to fall into the mass window around the Z(Z*) boson. Number of particle flow objects N_{PFO} in the event is required to be larger than a threshold value, which is affected and decided by the condition whether jets are originated from an on-shell Z boson or not, as well as to suppress backgrounds where the jets are reconstructed from any objects other than quark seeds coming from the Z boson. Cut on the polar angle of the sum of all visible particles $\cos\theta_{\mathrm{vis.}}$ is applied to further reject background processes, such as two-fermion components which tends to be back-to-back along the z axis. To reduce contamination of signal events belong to the other category, further requirement on recoil mass distribution is imposed at the final stage. Table 1 summaries the selection criteria applied across all the categories considered.

The signal and background reduction efficiencies as well as expected number of events running at $\sqrt{s} = 240$ GeV with an integrated luminosities of 5.6 ab^{-1} after the event selection are listed in the Table 2. In general, the analysis achieves a strong background rejection, while the signal selection efficiencies of approximately 30% and higher are kept. The main background which is common in all categories is the other Higgs decays. Four fermion processes, such as $e^+e^-\to\mathrm{ZZ}\to\mu\mu qq$ and $e^+e^-\to\mathrm{ZZ}\to\tau\tau qq$ due to the similarity of kinematics, have large contributions in the $qq\mathrm{H}\mu\mu\nu\nu$ category and in the $qq\mathrm{H}\nu\nu\mu\mu$ category, respectively.

For the BDT analysis, simpler selection criteria are applied prior to the BDT discrimination. The invariant and recoil mass of the associated Z boson which is reconstructed from di-objects (i.e. a pair of muons for $\mu\mu\mathrm{H}\nu\nu qq$ and $\mu\mu\mathrm{H}qq\nu\nu$ categories) are required to be in the region of the signal mass window. The selection requirements on the number of particle flow objects and the polar angle of the sum of all visible particles are also applied as used in the cut-based analysis.

A boosted decision tree is then trained on remaining signal and background events for each category separately. The boosting algorithm utilized in this analysis is the AdaBoost scheme [12]. The input variables to the BDT are defined as follows:

- $M_{\mu\mu}$, M_{jj}, $M_{\mathrm{miss.}}$: invariant mass of di-objects
- N_{PFO} : number of PFOs
- $\cos\theta_{\mathrm{vis.}}$, $\cos\theta$: polar angle of the sum of all visible particles
- $\Delta\phi_{\mathrm{ZZ}}$: angle between a Z boson reconstructed from the two muons and that reconstructed from the two jets
- $M_{\mathrm{jj}}^{\mathrm{recoil}}$, $M_{\mathrm{vis.}}$: recoil mass of the di-jets and invariant mass of all particles (for $\mu\mu\mathrm{H}\nu\nu qq/\mu\mu\mathrm{H}qq\nu\nu$ categories)
- $M_{\mathrm{jj}}^{\mathrm{recoil}}$, $M_{\mu\mu}^{\mathrm{recoil}}$: recoil mass of the di-jets and the di-muons (for $\nu\nu\mathrm{H}\mu\mu qq/\nu\nu\mathrm{H}qq\mu\mu$ categories)
- $M_{\mu\mu}^{\mathrm{recoil}}$, $M_{\mathrm{vis.}}$: recoil mass of the di-muons and invariant mass of all particles (for $qq\mathrm{H}\nu\nu\mu\mu/qq\mathrm{H}\mu\mu\nu\nu$ categories)
- $P_{\mathrm{vis.}}$, $P_{t,\mathrm{vis.}}$: magnitude of the momentum and transeverse momentum from summation of all visible particles
- $E_{\mathrm{j}}^{leading}$, $E_{\mathrm{j}}^{sub.}$: energy of the leading jet and the sub-leading jet
- $P_{t,\mathrm{j}}^{leading}$, $P_{t,\mathrm{j}}^{sub.}$: magnitude of transeverse momentum of the leading jet and the sub-leading jet

The final result of the BDT analysis exploits the increased sensitivity obtained by combining the 15 input variables into the final BDT discriminant. Fig. 2

Table 1 Overview of the requirements applied when selecting events (cut-based).

Pre-selections						
$N(l) = 2$, where leptons(l) should pass the isolation criteria $N(\mu^+) = 1$, $N(\mu^-) = 1$ with $E(\mu^\pm) > 3$ GeV $N(jet) = 2$						
Variable	$\mu\mu$H$\nu\nu qq$	$\nu\nu$H$\mu\mu qq$	$\nu\nu$H$qq\mu\mu$	qqH$\nu\nu\mu\mu$	qqH$\mu\mu\nu\nu$	$\mu\mu$H$qq\nu\nu$
$M_{\mu\mu}$ (GeV)	[80, 100]	[60, 100]	[10, 60]	[15, 55]	[75, 100]	[80, 100]
M_{jj} (GeV)	[15, 60]	[10, 55]	[60, 100]	[75, 105]	[75, 105]	[60, 105]
$M_{\mathrm{miss.}}$ (GeV)	[75, 105]	[75, 110]	[75, 110]	[70, 110]	[10, 50]	[10, 55]
$M_{\mu\mu}^{\mathrm{recoil}}$ (GeV)	[110, 140]	-	-	[175, 215]	[115, 155]	[110, 140]
$M_{\mathrm{vis.}}$ (GeV)	-	[110, 140]	[110, 140]	[115, 155]	[185, 215]	[175, 215]
$M_{\mathrm{jj}}^{\mathrm{recoil}}$ (GeV)	[185, 220]	-	-	[110, 140]	[110, 140]	-
N_{PFO}	[20, 90]	[20, 60]	[30, 100]	[40, 95]	[40, 95]	[30, 100]
$\lvert\cos\theta_{\mathrm{vis.}}\rvert$	< 0.95					
$\Delta\phi_{\mathrm{ZZ}}$ (degree)	[60, 170]	< 135	< 135	-	[120, 170]	[60, 170]
$\lvert M_{\mathrm{vis.}} - M_{\mathrm{H}}\rvert$ (GeV)	> 3	-	-	> 3	-	-
$\left\lvert M_{\mathrm{jj}}^{\mathrm{recoil}} - M_{\mathrm{H}}\right\rvert$ (GeV)	-	-	> 3	-	-	> 3
$\left\lvert M_{\mu\mu}^{\mathrm{recoil}} - M_{\mathrm{H}}\right\rvert$ (GeV)	-	> 3	-	-	> 3	-

Table 2 Summary of the selection efficiency ϵ and the number of expected events $\mathrm{N}_{evt.}$ for each category after the final event selection.

	$\mu\mu$H$\nu\nu qq$		$\nu\nu$H$\mu\mu qq$		$\nu\nu$H$qq\mu\mu$	
Process	ϵ [%]	$\mathrm{N}_{evt.}$	ϵ [%]	$\mathrm{N}_{evt.}$	ϵ [%]	$\mathrm{N}_{evt.}$
Signal	36	50	51	72	37	52
Higgs decays Bg.	$3.2{\cdot}10^{-3}$	36	$1.5{\cdot}10^{-3}$	17	$1.4{\cdot}10^{-2}$	159
SM four-fermion Bg.	$3.7{\cdot}10^{-6}$	4	$8.4{\cdot}10^{-6}$	9	$4.9{\cdot}10^{-5}$	52
SM two-fermion Bg.	0	0	0	0	0	0

	qqH$\nu\nu\mu\mu$		qqH$\mu\mu\nu\nu$		$\mu\mu$H$qq\nu\nu$	
Process	ϵ [%]	$\mathrm{N}_{evt.}$	ϵ [%]	$\mathrm{N}_{evt.}$	ϵ [%]	$\mathrm{N}_{evt.}$
Signal	30	42	25	35	34	48
Higgs decays Bg.	$2.9{\cdot}10^{-2}$	326	$1.8{\cdot}10^{-2}$	206	$6.8{\cdot}10^{-2}$	774
SM four-fermion Bg.	$1.8{\cdot}10^{-4}$	190	$2.8{\cdot}10^{-4}$	305	$6.1{\cdot}10^{-4}$	659
SM two-fermion Bg.	0	0	0	0	0	0

shows the obtained BDT score distributions for signal and background samples. For the final separation of signal and background events, the cut value on the BDT score is chosen so as to maximize a significance measure $S/\sqrt{S+B}$, where for a chosen cut, S(B) is the number of signal(background) events above this cut. The cut values as well as the other selection criteria are summrized in Table 3.

4 Result

Precision of the yield measurement of $\sigma_{ZH}\times$Br(H→ZZ) is estimated. The obtained signal and background distributions for recoil mass spectrum against the initial Z boson in the range 110-140 GeV, are added to make up a pseudo-experimental result, while the Probability Density Function (PDF) of both of the signal and the background are constructed individually by assuming the double-sided crystal ball distribution for the Higgs decays including the signals and the Gaussian for the SM processes. Note that the background is made of the Higgs decays except for the signal and the SM processes. The likelihood function is built from the the result as a observed events and PDFs as the number of expected events with the branching fraction Br(H→ZZ) only for the signal component being a free parameter and the maximum likelihood fitting is performed. A detail description can be found in Ref. [5]. The recoil mass distribution together with the fitting curves is shown in Fig. 3.

Table 4 summarizes the derived relative precision on the product of the ZH cross section and the branching ratio $\Delta(\sigma{\cdot}\mathrm{BR})/(\sigma{\cdot}\mathrm{BR})$, from the cut-based analysis and the BDT analysis. The bottom row shows the combined precision that is calculated from the standard error of the weighted mean, $\sigma = 1/\sqrt{\sum_{i=1}^{n}\sigma_i^{-2}}$, where σ_i is the uncertainty for each category. The systematic uncertainty is not taken into account in this result. Estimates of relative systematic uncertainty regarding to the pre-

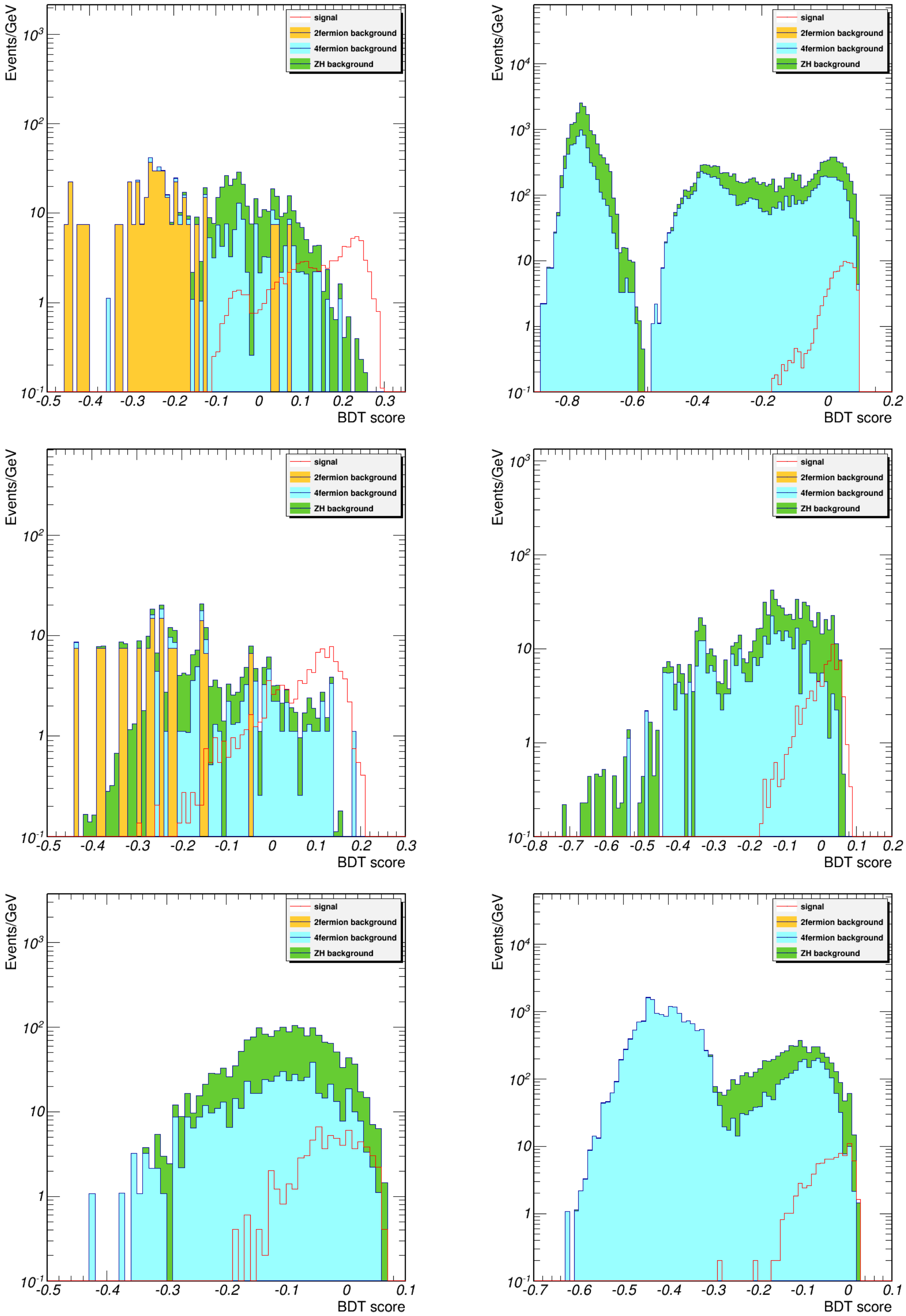

Fig. 2 (color online) BDT score distributions for 6 categories: $\mu\mu$H$\nu\nu qq$ (top left), $\mu\mu$H$qq\nu\nu$ (top right), $\nu\nu$H$\mu\mu qq$ (middle left), $\nu\nu$H$qq\mu\mu$ (middle right), qqH$\nu\nu\mu\mu$ (bottom left), and qqH$\mu\mu\nu\nu$ (bottom right). The signal distribution is shown with a red histogram while background contributions, ZH (green), 4-fermion (cyan) and 2-fermion (yellow), are drawn.

Table 3 Overview of the requirements applied when selecting events (BDT-based).

Pre-selections						
$N(l) = 2$, where leptons(l) should pass the isolation criteria						
$N(\mu^+) = 1$, $N(\mu^-) = 1$ with $E(\mu^\pm) > 3$ GeV						
$N(jet) = 2$						
Variable	$\mu\mu$H$\nu\nu qq$	$\mu\mu$H$qq\nu\nu$	$\nu\nu$H$\mu\mu qq$	$\nu\nu$H$qq\mu\mu$	qqH$\nu\nu\mu\mu$	qqH$\mu\mu\nu\nu$
$M_{\mu\mu}$ (GeV)	[80,100]		-	-	-	-
M_{jj} (GeV)	-	-	-	-	[75, 105]	[75,110]
$M_{\mathrm{miss.}}$ (GeV)	-	-	[75, 110]		-	-
$M_{\mu\mu}^{\mathrm{recoil}}$ (GeV)	[110, 140]		-	-	-	-
$M_{\mathrm{vis.}}$ (GeV)	-	-	[110, 140]		-	-
$M_{\mathrm{jj}}^{\mathrm{recoil}}$ (GeV)	-	-	-	-	[110, 140]	
N_{PFO}	[20, 90]	[30, 100]	[20, 60]	[30, 100]	[40, 95]	[35, 100]
$\|\cos\theta_{\mathrm{vis.}}\|$	< 0.95					
BDT score	> 0.15	> 0.03	> -0.01	> 0.00	> -0.05	> -0.02

cision measurement of σ_{ZH} at the CEPC is described in Ref. [10] and that's would be a base for the future study of the systematic uncertainty. The final result for the relative statistical uncertainty of the $\sigma_{ZH}\times$Br(H$\to$ZZ) is estimated to be 9.71% in the cut-based analysis and 8.80% in the BDT analysis.

Table 4 Statistical uncertainties on the product of the ZH cross section and the branching ratio. The bottom row shows the result of combined value of the 6 categories.

Channel		$\frac{\Delta(\sigma \cdot BR)}{(\sigma \cdot BR)}$ [%] cut-based	BDT
$Z\to\mu^+\mu^-$	$H\to ZZ^*\to\nu\bar{\nu}q\bar{q}$	18.1	15.8
$Z\to\mu^+\mu^-$	$H\to ZZ^*\to q\bar{q}\nu\bar{\nu}$	65.4	58.2
$Z\to\nu\bar{\nu}$	$H\to ZZ^*\to\mu^+\mu^-q\bar{q}$	13.5	13.1
$Z\to\nu\bar{\nu}$	$H\to ZZ^*\to q\bar{q}\mu^+\mu^-$	27.7	23.6
$Z\to q\bar{q}$	$H\to ZZ^*\to\mu^+\mu^-\nu\bar{\nu}$	63.5	46.1
$Z\to q\bar{q}$	$H\to ZZ^*\to\nu\bar{\nu}\mu^+\mu^-$	54.3	45.2
Combined		9.71	8.80

Finally, the precision of the Higgs boson width is estimated by combining the obtained final precision of the signal yield and the the precision of σ_{ZH} measurement of 0.5% [5]. From the cut-based analysis, the relative precision of the Higgs width is estimated to be 9.73% whereas it is 8.82% from the BDT analysis.

5 Summary

The precision of the yield measurement $\sigma_{ZH}\times$Br(H$\to$ZZ) at the CEPC is evaluated using MC samples for the baseline concept running at $\sqrt{s} = 240$ GeV with an integrated luminosities of 5.6 ab^{-1}. Among the various decay modes of the H$\to$ZZ, the signal process having two muons, two jets and missing momentum in final states has been chosen. After the event selection, relative precision is evaluated with the likelihood fitting method on signal and background. The final value combined from all of six categories is 9.71% from the cut-based analysis and 8.80% from the BDT analysis. The relative precision of the Higgs boson width, using this H$\to$ZZ decay, is estimated by combining the obtained result with the precision of the inclusive ZH cross section and it is estimated to be 8.82% from the BDT analysis.

Acknowledgements The authors would like to thank the CEPC computing team for providing the simulation tools and samples. We also thank Yaquan Fang, Manqi Ruan, Gang Li, and Yuhang Tan for helpful discussions.

References

1. ATLAS Collaboration, G. Ada *et al.*, Observation of a new particle in the search for the Standard Model Higgs boson with the ATLAS detector at the LHC, Phys. Lett. B, **716**, 1-29 (2012), arXiv:1207.7214 [hep-ex]
2. CMS Collaboration, S. Chatrchyan *et al.*, Observation of a new boson at a mass of 125 GeV with the CMS experiment at the LHC, Phys. Lett. B, **716**, 30-61 (2012), arXiv:1207.7235 [hep-ex]
3. The CEPC Study Group, CEPC Conceptual Design Report: Volume 1 - Accelerator (2018), arXiv:1809.00285 [physics.acc-ph]
4. The CEPC Study Group, CEPC Conceptual Design Report: Volume 2 - Physics & Detector (2018), arXiv:1811.10545 [hep-ex]
5. F. An *et al.*, Precision Higgs physics at the CEPC, Chinese Physics C **43** no.4 (2019) 043002
6. T. Behnke *et al.*, The International Linear Collider Technical Design Report - Volume 4: Detectors (2013), arXiv:1306.6329 [physics.ins-det]
7. W. Kilian, T. Ohl, and J. Reuter, WHIZARD simulating multi-particle processes at LHC and ILC, Eur. Phys. J. C **71**, 1742 (2011), arXiv:0708.4233 [hep-ph]
8. P. Mora de Freitas and H. Videau, Detector simulation with MOKKA/GEANT4: Present and future, Presented at the International Workshop

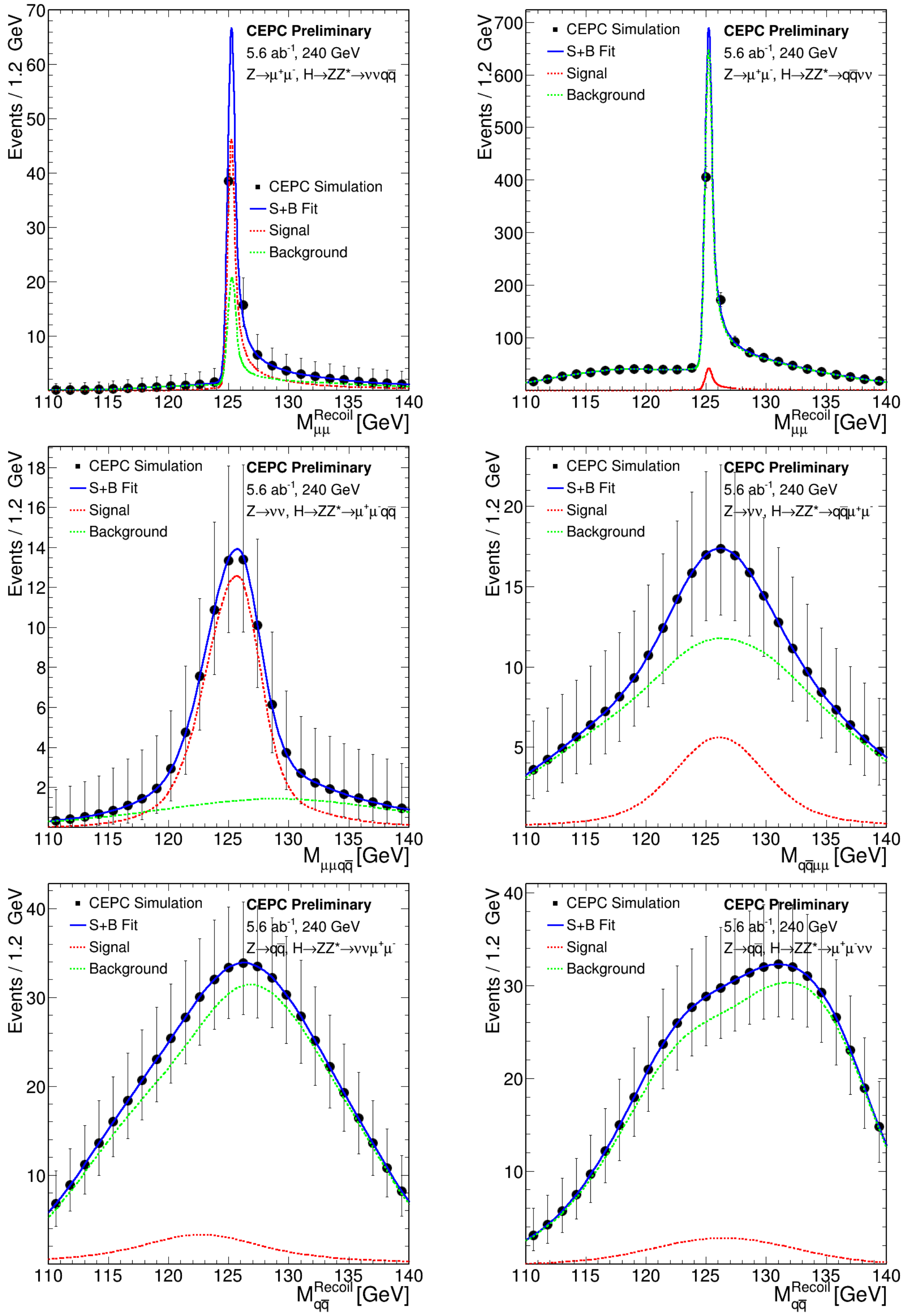

Fig. 3 (color online) Recoil mass distributions for each category. The black dots represent the predicted results at the CEPC and the solid blue line shows the fitting curve which is broken down into signal (dashed red line) and background (dashed green line) components.

on Linear Colliders (LCWS 2002), 623-627 (2002), https://inspirehep.net/literature/609687

9. M. Ruan *et al.*, Reconstruction of physics objects at the Circular Electron Positron Colluder with Arbor, Eur. Phys. J. C **78** 426 (2018)
10. Z. Chen *et al.*, Cross section and Higgs mass measurement with Higgsstrahlung at the CEPC, Chinese Physics C **41** no.2 (2017) 023003
11. Pedregosa *et al.*, Scikit-learn: Machine Learning in Python, JMLR 12, pp. 2825-2830, (2011)
12. Y. Freund, and R. Schapire, A Decision-Theoretic Generalization of On-Line Learning and an Application to Boosting, Journal of Computer and System Sciencesss, **55**, 119-139, (1997)